Supplementary Information for Atomic ribbons formation in pulsed laser patterning of WS_2 layers

Yaowu Hu [a, b†], Zifeng Wang [a], Zequn Zhang [a], Jie Guan [c]

[a] The Institute of Technological Sciences, Wuhan University, Wuhan, 430072, China

[b] School of Power and Mechanical Engineering, Wuhan University, 430072 Wuhan, China

[c] School of Physics, Southeast University, Nanjing, 211189, China

[†] Corresponding author.

E-mail: yaowuhu@whu.edu.cn

TEL: +86-13387587827

Experimental method

Wet transfer

First, a 90 mg/mL polystyrene (PS) solution was equipped with polystyrene as solute and toluene solution as solvent. Afterwards, the PS solution was spin-coated on the WS_2 surface of the sapphire substrate and baked at 80 °C for 2 minutes. The PS film containing WS_2 was obtained by stripping in water after simple micro processing around the sample. Clean wafers were taken to fish the PS films out of the water and dried. After that, the film was baked at 110°C for half an hour to make the contact between the film and the wafer closer. Finally, the wafers were put into toluene solution for about 2 minutes and then pulled out, and the transfer was completed.

Simulation method

Molecular dynamics (MD) simulation

MD simulations were performed using the LAMMPS code[1]. In the simulations, the Stillinger Weber (SW) potential is used to describe the interatomic interactions in monolayer WS_2. the interactions between Si and WS_2 are described by the Lennard-Jones potential. The isothermal isobaric system (NVT) was used for the relaxation of the initial test system at a temperature of about 300 K and a relaxation time of 10 ps. The MD simulations were performed using a micro-regular system synthesis (NVE) with a ramp-up command of fix ehex. The simulation time step was set to 1 fs. Ovito

software was used for the structure visualization.

Density Functional Calculations

Density functional theory (DFT) was used for the electronic structure calculations as implanted in the Vienna ab initio simulation package (VASP)[2]. The projector augmented wave (PAW) method was used to describe the potential between ionic cores and electrons[3]. The exchange-correlation functional was decided by the generalized gradient approximation (GGA) in the Perdew-Burke-Ernzerhof (PBE) parametrization[4]. Band structure was calculated along the symmetry points Γ, X, S, Y, Γ. The k-point sampling for the first Brillouin zone was done with a 8×8×1 Γ-centered k-points grid in a unit cell or its equivalence in the supercells[5]. The energy cutoff was set to 500 eV for all cases. All the geometries were optimized using the conjugated-gradient method[6] and a Hellman-Feynman force convergent tolerance of 10^{-3} eV/Å was set. The energy differences are converged within 10^{-6} eV for each electronic self-consistency iteration. To simulate the low-dimensional systems, a vacuum region is set in excess of 25 Å between isolated structures.

Finite-Difference Time-Domain Calculations

The electromagnetic field strength of the atomic WS_2 layers was simulated using commercial Lumerical FDTD software. In the simulation setup, the SEM images obtained from the experiments were binarised and imported into the software. For single-layer WS_2 and few-layer WS_2 samples, the structural model settings chosen were: the length and width were kept the same at 2 μm, and the height distribution was set to 1 nm and 3 nm and placed on a SiO_2/Si substrate.

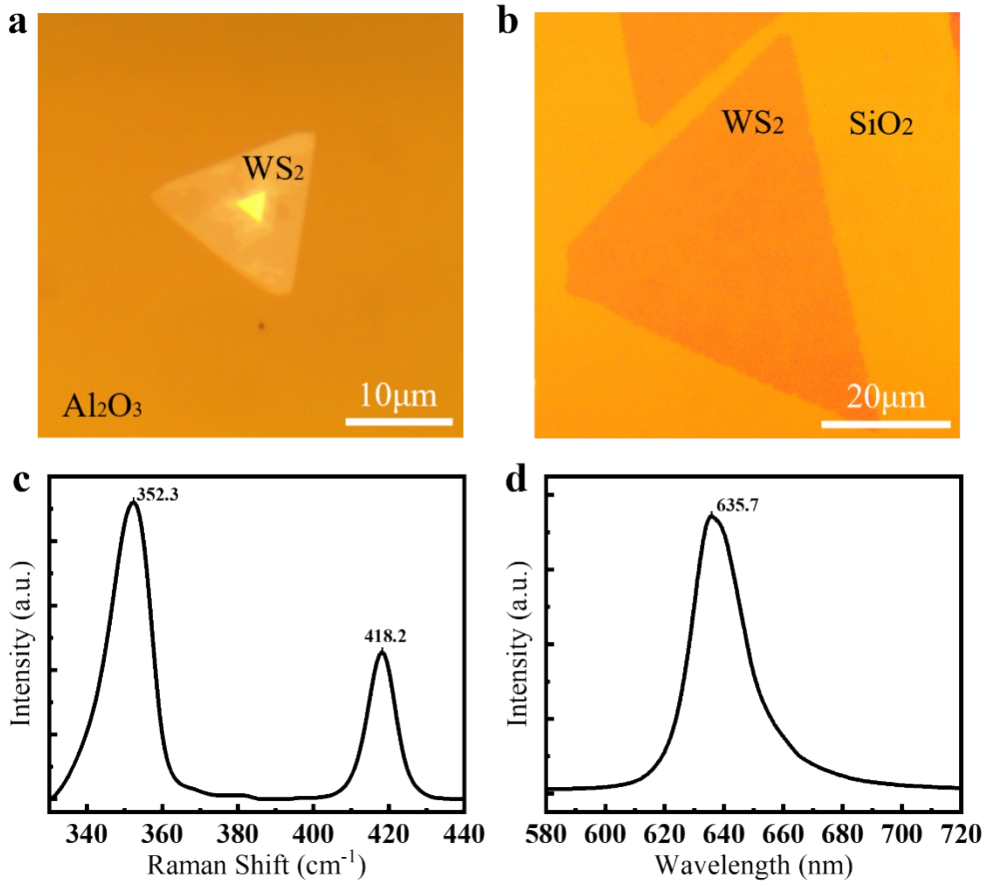

Fig. S1 (a) Optical microscope photograph of WS_2 grown by CVD on a substrate with Al_2O_3. **(b)** Optical microscope photo of WS_2 transferred onto a silicon substrate with a 300 nm oxide layer by wet transfer technique. **(c)** Raman spectrum and **(d)** PL spectrum of WS_2 measured by 532nm excitation laser.

The growth of WS_2 is evidenced by the location of the E^1_{2g} and A_{1g} peaks of WS_2 in Fig. S1(c) at 352.3 cm and 418.2 cm, respectively[7]. The PL peak of WS_2 in Fig. S1(d) is 635.7 nm, which corresponds to a band gap of 1.95 eV, indicating that WS_2 is a monolayer[8].

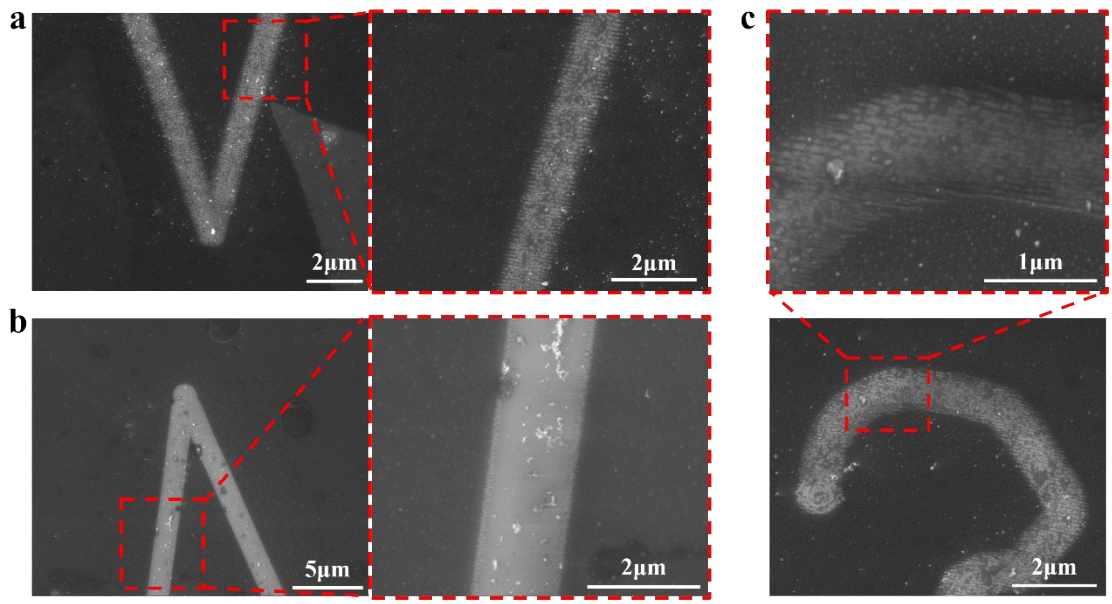

Fig. S2 Effects of laser processing path changes on atomic-level LIPSS. **(a)** SEM results of laser subtractive processing of atomic layer WS_2 using different mathining paths. **(b)** SEM results of laser subtractive machining of atomic layer MoS_2 using different machining paths. **(c)** Laser subtractive machining results of atomic layer WS_2 with curved machining path.

When femtosecond laser subtractive machining the atomic layer WS_2, the direction of the atomic-level nanoribbons does not change with the change of the laser path, as shown in Fig S2(a). Femtosecond laser subtractive machining of atomic layer MoS_2 will not produce atomic-level nanoribbons in the processing area, as shown in Fig S2(b). In addition, from Fig S2(c), it can be found more clearly that the generation of atomic-level LIPSS is caused by the polarization of the laser, because the direction of the atomic-level nanoribbons is always consistent, that is, perpendicular to the direction of laser polarization.

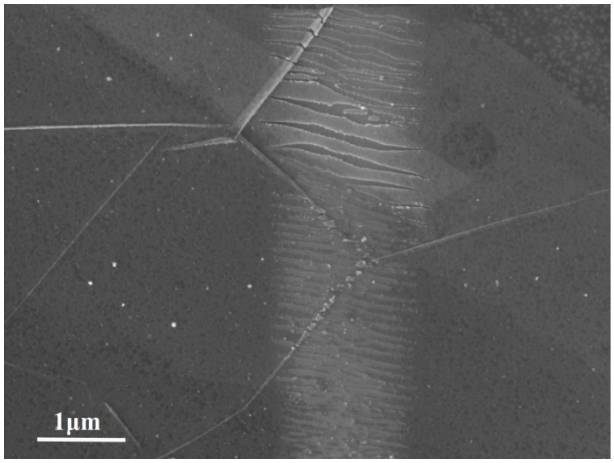

Fig. S3 SEM images of multilayer and monolayer coexisting WS_2 films after femtosecond laser removal, laser wavelength 1060 nm, pulse width 190 fs, energy 0.6 mW.

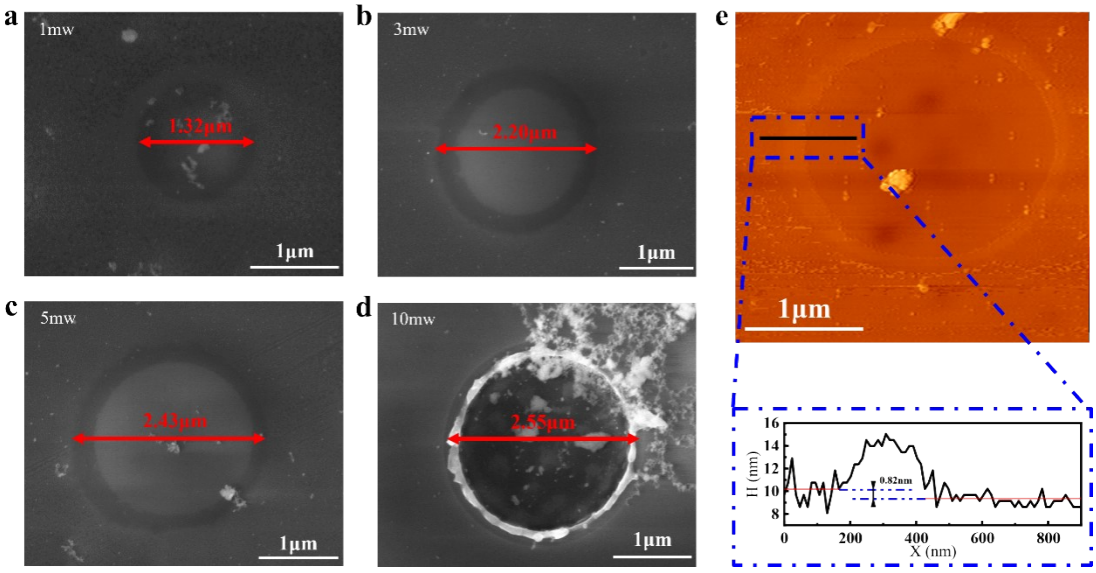

Fig. S4 SEM images of a laser with wavelength of 1064 nm and pulse width of 190 fs machining of monolayer of WS_2 under different power conditions. **(a)** Results of laser machining monolayer of WS_2 at 1 mW. **(b)** Results of laser machining monolayer of WS_2 at 3 mW. **(c)** Results of laser machining monolayer of WS_2 at 5 mW. **(d)** Results of laser machining monolayer of WS_2 at 10 mW. **(e)** Morphology and thickness measurements of a monolayer of WS_2 measured using AFM.

As the laser power increases, the area of the monolayer WS2 removed gradually increases, as shown in the Fig. S4(a) (b) (c). The substrate is damaged when the laser

energy is too high, as shown in Fig. S4(d). The measured position in Fig. S4(e) shows the WS_2 boundary after femtosecond laser machining, and the result proves that WS_2 is a monolayer[9].

References

[1] S. PLIMPTON, FAST PARALLEL ALGORITHMS FOR SHORT-RANGE MOLECULAR DYNAMICS, J. Comput. Phys. 117 (1995) 1–19. https://doi.org/10.1039/c7sm02429k.

[2] G. Kresse, J. Furthmüller, Efficient iterative schemes for ab initio total-energy calculations using a plane-wave basis set, Phys. Rev. B - Condens. Matter Mater. Phys. 54 (1996) 11169–11186. https://doi.org/10.1103/PhysRevB.54.11169.

[3] P.E. Blöchl, Projector augmented-wave method, Phys. Rev. B. 50 (1994) 17953–17979. https://doi.org/10.1103/PhysRevB.50.17953.

[4] J.P. Perdew, K. Burke, M. Ernzerhof, Generalized gradient approximation made simple, Phys. Rev. Lett. 77 (1996) 3865–3868. https://doi.org/10.1103/PhysRevLett.77.3865.

[5] J.D. Pack, H.J. Monkhorst, "special points for Brillouin-zone integrations"-a reply, Phys. Rev. B. 16 (1977) 1748–1749. https://doi.org/10.1103/PhysRevB.16.1748.

[6] M.R. Hestenes, E. Stiefel, Methods of Conjugate Gradients for Solving, J. Res. Natl. Bur. Stand. (1934). 49 (1952) 409–436.

[7] A. Berkdemir, H.R. Gutiérrez, A.R. Botello-Méndez, N. Perea-López, A.L. Elías, C.I. Chia, B. Wang, V.H. Crespi, F. López-Urías, J.C. Charlier, H. Terrones, M. Terrones, Identification of individual and few layers of WS_2 using Raman Spectroscopy, Sci. Rep. 3 (2013) 1–8. https://doi.org/10.1038/srep01755.

[8] A.L. Elías, N. Perea-López, A. Castro-Beltrán, A. Berkdemir, R. Lv, S. Feng, A.D. Long, T. Hayashi, Y.A. Kim, M. Endo, H.R. Gutiérrez, N.R. Pradhan, L. Balicas, T.E. Mallouk, F. López-Urías, H. Terrones, M. Terrones, Controlled synthesis and transfer of large-area WS_2 sheets: From single layer to few layers,

ACS Nano. 7 (2013) 5235–5242. https://doi.org/10.1021/nn400971k.

[9] C. Lan, Z. Zhou, Z. Zhou, C. Li, L. Shu, L. Shen, D. Li, R. Dong, Wafer-scale synthesis of monolayer WS_2 for high- performance flexible photodetectors by enhanced chemical vapor deposition, Nano Res. 11 (2018) 3371–3384. https://doi.org/10.1007/s12274-017-1941-4.